AD-A207 123

SC5508.APR

Copy No. 3

ENVIRONMENTAL INTEGRITY OF COATING/METAL INTERFACE

ANNUAL PROGRESS REPORT FOR THE PERIOD
February 1, 1988 through January 31, 1989

CONTRACT NO. N00014-87-C-0075

Prepared for

Scientific Officer
Metallic Materials Division, Code 1131M
Office of Naval Research
800 North Quincy Street
Arlington, VA 22217

Att: Dr. A. John Sedriks

M. Kendig
Program Manager

DTIC
ELECTE
APR27 1989
S H D

MARCH 1989

Approved for public release; distribution is unlimited

Rockwell International
Science Center

089 4 23 104

REPORT DOCUMENTATION PAGE

FORM APPROVED
OMB No. 0704-0188

1a. REPORT SECURITY CLASSIFICATION
UNCLASSIFIED

1b. RESTRICTIVE MARKINGS

2a. SECURITY CLASSIFICATION AUTHORITY

3. DISTRIBUTION/AVAILABILITY OF REPORT
Approved for public release; distribution is unlimited

2b. CLASSIFICATION/DOWNGRADING SCHEDULE

4. PERFORMING ORGANIZATION REPORT NUMBER(S)
SC5508.APR

5. MONITORING ORGANIZATION REPORT NUMBER(S)

6a. NAME OF PERFORMING ORGANIZATION
ROCKWELL INTERNATIONAL
Science Center

6b. OFFICE SYMBOL *(If Applicable)*

7a. NAME OF MONITORING ORGANIZATION

6c. ADDRESS *(City, State, and ZIP Code)*
1049 Camino Dos Rios
Thousand Oaks, CA 91360

7b. ADDRESS *(City, State and ZIP Code)*

8a. NAME OF FUNDING/SPONSORING ORGANIZATION
Scientific Officer
Office of Naval Research

8b. OFFICE SYMBOL *(If Applicable)*

9. PROCUREMENT INSTRUMENT IDENTIFICATION NUMBER
CONTRACT NO. N00014-87-C-0075

8c. ADDRESS *(City, State and ZIP Code)*
800 North Quincy St.
Arlington, VA 22217-5000

10. SOURCE OF FUNDING NOS.

PROGRAM ELEMENT NO.	PROJECT NO.	TASK NO.	WORK UNIT ACCESSION NO.

11. TITLE *(Include Security Classification)*
ENVIRONMENTAL INTEGRITY OF COATING/METAL INTERFACE

12. PERSONAL AUTHOR(S)
Kendig, M., Stocker, P., Lumsden J.

13a. TYPE OF REPORT	13b. TIME COVERED	14. DATE OF REPORT *(Year, Month, Day)*	15. PAGE COUNT
Annual Progress Report	FROM **02/01/88** TO **01/31/89**	**1989, MARCH**	

16. SUPPLEMENTARY NOTATION

17. COSATI CODES			18. SUBJECT TERMS *(Continue on reverse if necessary and identify by block number)*
FIELD	GROUP	SUB-GROUP	

19. ABSTRACT *(Continue on reverse if necessary and identify by block number)*

20. DISTRIBUTION/AVAILABILITY OF ABSTRACT
UNCLASSIFIED/UNLIMITED ☐ SAME AS RPT. ☐ DTIC USERS ☒

21. ABSTRACT SECURITY CLASSIFICATION
UNCLASSIFIED

22a. NAME OF RESPONSIBLE INDIVIDUAL	22b. TELEPHONE NUMBER *(Include Area Code)*	22c. OFFICE SYMBOL
Dr. A. John Sedriks		

DD FORM 1473, JUN 86 **Previous editions are obsolete.**

TABLE OF CONTENTS

		Page
1.0	ABSTRACT	1
2.0	SCOPE AND OBJECTIVES	2
3.0	EXPERIMENTAL	4
3.1	Preparation of the Coated Steel	4
3.2	Wetting Experiments	4
3.3	Surface Analysis	5
4.0	SUMMARY OF RESULTS AND PROGRESS	8
4.1	Scanning Acoustic Microscopy	8
4.2	Potential-Dependent Surface Energy of Steel Under Cathodic Disbond Conditions	11
4.3	Surface Analysis of Cathodicallyh Polarized Steel Surfaces in Alkaline Environments	18
5.0	SUMMARY	28
6.0	FUTURE WORK	29

DTIC COPY INSPECTED 4

Accession For
NTIS GRA&I ☑
DTIC TAB ☐
Unannounced ☐
Justification
By
Distribution/
Availability Codes
Dist | Avail and/or Special
A-1

LIST OF FIGURES

Figure		Page
1	Schematic for in situ scanning acoustic microscopy.....	3
2	Schematic for the apparatus used to obtain wetting force vs potential data.	5
3	Schematic for the in situ cell used to prepare samples for analysis in the UHV chamber: (a) details of chamber, (b) details of the chemical/electrochemical conditioning system.	7
4	Potential dependence of the disbonding rate constant, K_d.	8
5	Acoustic micrograph illustrating alteration of the hydroxy-terminated polybutadiene by exposure to 1.0 M NaOH.	10
6	Model for the polymer degradation process.....	10
7	Schematic showing the forces present during the wetting balance experiment.	14
8	Potential dependence for (a) the wetting tension, γ, and (b) the current density of steel in 0.5 M NaCl. The potential was varied at a constant rate of 0.5 mV/s from just above the open circuit potential to -1000 mV.....	15
9	Change in the wetting tension, $\Delta\gamma$, as a function of cathodic polarization in 0.5 M NaOH for two HCl-etched steel specimens.	16
10	pH dependence for the potential E_w where accelerated wetting occurs.	16
11	Change in wetting tension, $\Delta\gamma$, and potential, E as a function of time during galvanic polarization of mild steel in pH 9.6 borate buffer: (a) sample etched in HCl, (b) sample prepolarized for 3.7 min. at 0 V vs Ag/AgCl in the 0.1 M pH 9.6 borate buffer.	18
12	Auger electron spectrum for (a) a polished and air aged steel specimen before exposure to 1 M NaOH and (b) after ion etching	20

LIST OF FIGURES (continued)

Figure		Page
13	Auger electron spectrum for a polished and air aged steel specimen after exposure to deaerated 1 M NaOH.	21
14	Oxygen 1s X-ray photoelectron spectrum for the specimen of Fig. 13.	21
15	Iron 2p X-ray photoelectron spectrum for the specimen of Fig. 13.	22
16	Oxygen 1s X-ray photoelectron spectrum for steel exposed to deaerated 1.0 M NaOH at -745 mV vs SCE (-700 mV vs Ag/AgCl).	23
17	Iron 2p X-ray photoelectron spectrum for steel exposed to deaerated 1.0 M NaOH at -745 mV vs SCE (-700 mV vs Ag/AgCl).	23
18	Oxygen 1s X-ray photoelectron spectrum for steel exposed to deaerated 1.0 M NaOH at -1032 mV vs SCE (-987 mV vs Ag/AgCl).	24
19	Iron 2p X-ray photoelectron spectrum for steel exposed to deaerated 1.0 M NaOH at -1032 mV vs SCE (-987 mV vs Ag/AgCl).	24
20	Intensity ratio for the Fe/Si Auger lines as a function of the time of Ar ion etching for the sample exposed to 0.001 M NaOH at -1000 mV vs SCE (-955 mV vs Ag/AgCl).	25
21	Iron 2p X-ray photoelectron spectrum for steel exposed to deaerated 0.001 M NaOH at -1000 mV vs SCE (-955 mV vs Ag/AgCl).	26
22	Oxygen 1s X-ray photoelectron spectrum for steel exposed to deaerated 0.001 M NaOH at -1000 mV vs SCE (-955 mV vs Ag/AgCl).	26
23	Energy for the maximum in the low energy peak of the Fe oxide 1s X-ray photoelectron spectrum as a function of polarization in the in situ cell.	27

1.0 ABSTRACT

It is the objective of this project to establish the molecular details of the corrosion-induced loss of adhesion of organic films from steel. Scanning acoustic microscopy (SAM) has allowed observation of the microscopic details of the attack of cathodic corrosion products on a model organic coating on steel. Attack of the polymer by the alkaline corrosion products occurs at numerous localized regions resulting in the mechanical degradation of the coating/metal interface. Acoustic microscopy has also provided a rapid determination of the kinetics of the disbonding process. The disbond distance away from a cathodically polarized scribe increases with the square root of time. The corresponding rate parameter K_d' increases with decreasing potential for applied potentials below -750 mV vs Ag/AgCl.

A modified Wilhelmy balance was used to determine the relative hydrophilicity of steel as a function of potential. The results demonstrate that steel at pH 9.6 becomes dramatically more hydrophilic for potentials cathodic to -750 mV vs Ag/AgCl as a result of the reduction of the native Fe_2O_3 oxide. Preliminary surface analyses also suggest a reduction of the oxidic surface at potentials and pH conditions corresponding to those within the crevice formed by a cathodic disbond.

2.0 SCOPE AND OBJECTIVES

Adhesion or maintenance of an intimate molecular contact between a low dielectric constant, nonconducting organic films and a metal substrate diminishes the rate of corrosion of the metal despite the apparent facility of corrodents such as oxygen and ionic solutes to permeate the organic matrix. It is the objective of this project to understand the corrosion-induced degradation of adhesion of organic coating/metal systems. It is anticipated that understanding the fundamentals of corrosion-induced adhesion loss will lead to concepts for improving the resistance of the polymer/steel interface to corrosive degradation. This program has three tasks directed toward the following goals:

1. Characterization of the kinetics of failure at the organic coating/steel interface.
2. Determination of the molecular events at the steel/polymer/environment interface that lead to adhesion loss
3. Evaluation of the relative strength of acid/base interaction of polymers with iron and steel surfaces in the presence of charge and mass flux associated with the electrochemical reactions of corrosion.

In the previous year of this program, effort was directed toward Task 1. During the period of this report, effort has been directed toward Tasks 1 and 2. The evaluation of kinetics (Task 1) using novel acoustic microscopy (Fig. 1) has been completed and reported.[1-5] Additional information from acoustic microscopy has allowed completion of a macroscopic picture for the cathodic disbonding of a model hydroxy-terminated polybutadiene from a mild steel substrate.

In order to understand the molecular aspects of the polymer/substrate oxide interactions, baseline information on the oxides present in a model cathodic disbonded environment and the role these oxides play on the relative ability of the aqueous phase to displace the organic polymer film has been obtained during the period covered by this report. The experimental approach for characterizing the chemistry of the surface of cathodically polarized steel in alkaline environments entailed the use of an in situ cell

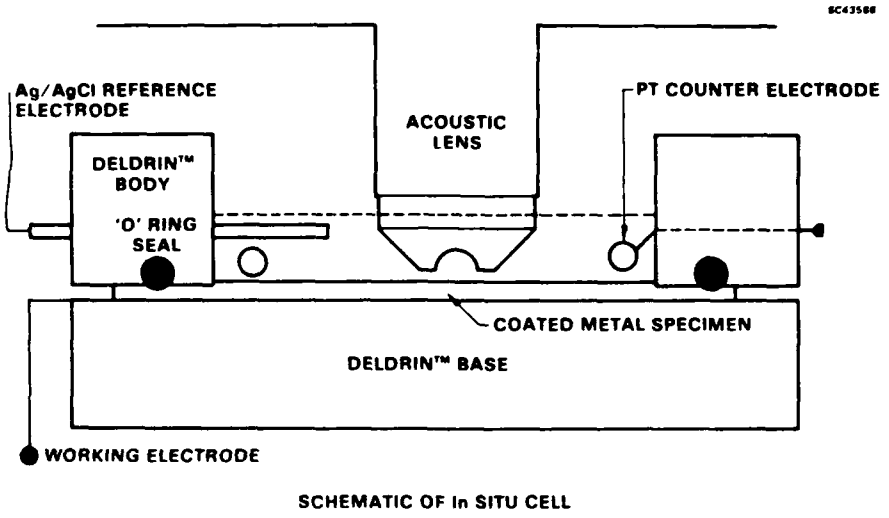

Fig. 1 Schematic of in situ scanning acoustic microscopy.

for preparing specimens for analysis in UHV using the highly surface sensitive techniques of x-ray photoelectron spectroscopy (XPS) and Auger electron spectroscopy (AES). A highly sensitive wetting balance that allowed simultaneous electrochemical polarization and wetting force measurements characterized the role of electrochemical potential on the relative hydrophilicity of steel surfaces. The relative hydrophilicity of the steel relates to the energy required for an aqueous phase to displace the nonpolar adherent organic film. The results lead to a preliminary hypothesis for the molecular interactions involved in cathodic disbonding of organic polymer coatings from steel.

3.0 EXPERIMENTAL

3.1 Preparation of the Coated Steel

A filtered (0.2 μm) solution containing four parts of hydroxy-terminated polybutadiene (PBOH) (R45HT from the Sartomer Co.) in three parts mineral spirits containing Modiflow™ (0.1% by weight of active ingredients) were spin coated on polished and degreased 0.055 cm thick 1010 steel coupons. The steel polished with 600 grit SiC paper was wiped with a towel moistened with acetone and degreased in hexane before applying the coating. Wet-coated samples were air dried for 12 h and oxidatively cross-linked by curing in a oven reaching 205°C for 9 min. The resulting coatings had a nominal 4 μm thickness. Several additional pretreatments included a nitric acid oxidation (HNO_3) and a cleaning in inhibited HCl (inh HCl) as described previously[6,7] in addition to treatment in an iso-propanolic solution of Kenrich LICA #38. In one case, the LICA #38 was included in the coating solution.

The resulting coupons were scribed (2.5 cm perpendicular marks using a SiC tool) and placed with the scribe mark to the electrolyte in the in situ acoustic microscope cell (Fig. 1). In this manner, the specimens could be polarized to different cathodic potentials and monitored acoustic microscopically as a function of time. A region adjacent to the scribe mark which was parallel to the 600 grit polishing scratches was monitored as a function of time.

3.2 Wetting Experiments

The wettability of steel by neutral and alkaline electrolytes was observed as a function of potential using the apparatus shown in Fig. 2. This apparatus allowed measurement of the wetting forces on the steel specimen as a function of applied cathodic potential. 1010 steel cylinders, having a typical 0.077 cm radius, were polished with 600 grit SiC paper and etched for 30 s in concentrated HCl followed by a thorough rinse in distilled water and drying before mounting on the wetting balance shown schematically in Fig. 2. The cylinder specimen was immersed to a depth of approximately 0.05 cm and allowed to equilibrate with the electrolyte until the change in the wetting tension $\Delta\gamma$ remained constant at which point the potential was ramped at a rate

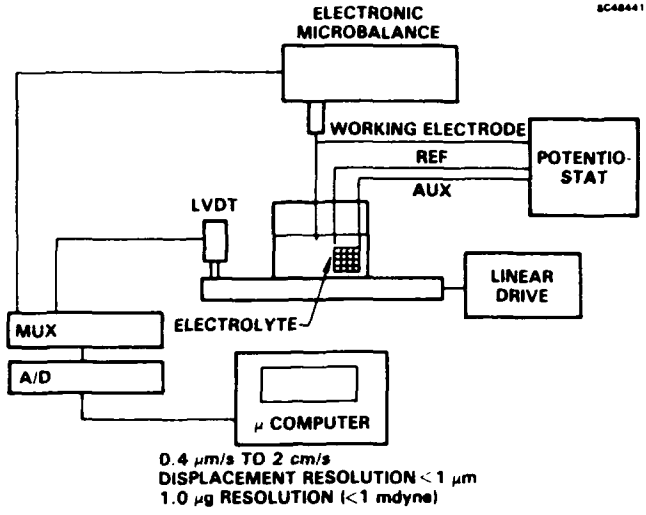

Fig. 2 Schematic for the apparatus used to obtain wetting force vs potential data.

of 0.5 mV/s from approximately the open circuit potential to -1100 mV vs a Ag/AgCl reference electrode. Alternatively, or the sample was polarized galvanostatically with a cathodic current of typically 100-200 $\mu A/cm^2$ while recording both the wetting force and potential. This method for wetting tension measurement is often referred to as the Wilhelmy plate method and has been reported previously as a viable method for characterizing electrochemically governed wetting.[13,14a] The solutions used in this study appear in Table I.

3.3 Surface Analysis[8]

Figure 3(a) shows the in situ cell used to prepare specimens for direct transfer to the UHV chamber for surface analysis. The cell is mounted on a 20 cm stainless steel flange so that it extends into the UHV chamber and is constructed from titanium and glass-filled teflon. The solution or water rinses can be admitted and expelled from an exterior reservoir system the details of which appear in Fig. 3(b). There is a small circular opening between the cell and the UHV chamber for inserting the sample. The opening can be vacuum sealed from within the cell by a movable plug and can be sealed from within the UHV chamber with the sample. A saturated calomel reference electrode is used to measure the potential.

Table 1

Solutions

Solute(s)	Concentration(s)	pH
NaCl	0.5 M	6.1
NaOH	0.5 M	~ 13.5
NaCl/NaOH	0.5 M/0.05 M	12.4
NaCl/NaOH	0.5 M/0.005 M	11.45
NaCl/NaOH	0.5 M/0.0005 M	10.13
NaCl/NaOH	0.5 M/0.00005 M	8.08
H_3BO_3	0.1 M pH adjusted to 9.6 with NaOH	

By means of a movable plug, the cell is closed to the chamber and is evacuated independently of the UHV system. After achieving UHV, the sample is inserted into the cell opening and gripped in place. Solution is then admitted into the cell from the external reservoir and the plug is retracted to cause immersion of the sample in solution. With valves A and P (the plug) open (Fig. 3(b)), the sample can be polarized or its potential measured using the cell wall as the counter electrode. When the sample has been exposed to the solution the desired length of time under controlled potential or current conditions, the electrolyte is drained, and rinsed if desired and the remaining liquid is pumped using a sorption pump-trap apparatus; the plug is then inserted from the inside of the cell. The plug and sample surfaces are separated by ~ 0.2 mm when both are inserted. The sample is next removed for analysis.

The sample used for this experiment was a 1010 carbon steel which was Ar etched and equilibrated with air before exposing to the electrolytic conditioning.

Further details of the electron optics and procedures for the use of the cell appear elsewhere.[8]

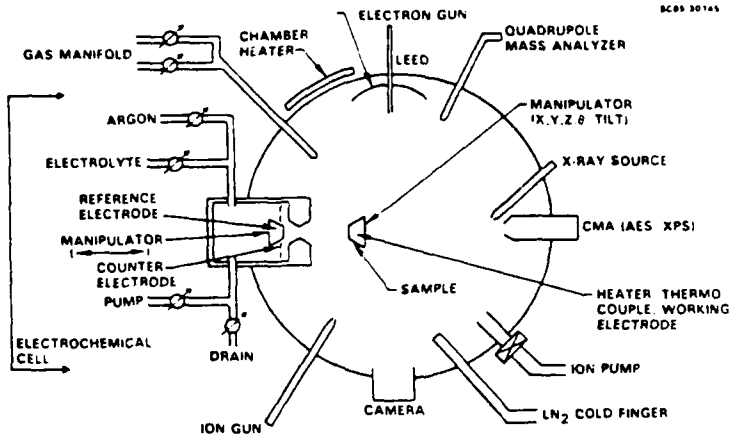

(a)

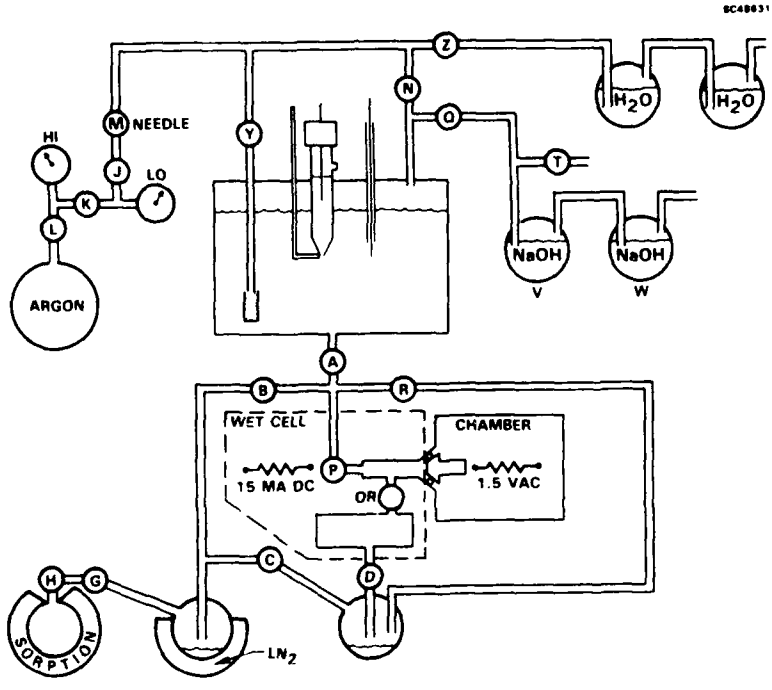

(b)

Fig. 3 Schematic for the in situ cell used to prepare samples for analysis in the UHV chamber: (a) details of the chamber, (b) details of the chemical/electrochemical conditioning system.

4.0 SUMMARY OF RESULTS AND PROGRESS

4.1 Scanning Acoustic Microscopy (SAM)

Most of the SAM work was completed in the previous contract year.[1-5] However, additional work was performed this year to complete a picture of the cathodic disbonding process. As observed previously the cathodic disbonding was associated with a distribution of circular features referred to as "microblisters".[1-5] The movement of the disbond front follows a rate law:

$$d = d_o + K_d\sqrt{t} \qquad (1)$$

where d is the distance the disbond front has moved from the scribe mark. The rate constant K_d depends on potential as shown in Fig. 4. A dramatic increase in K_d occurs for potentials more negative than -750 mV vs Ag/AgCl (-795 mV vs SCE). This rapid rise at a specific potential suggest an electrochemical reaction is involved in the initiation of cathodic disbonding.

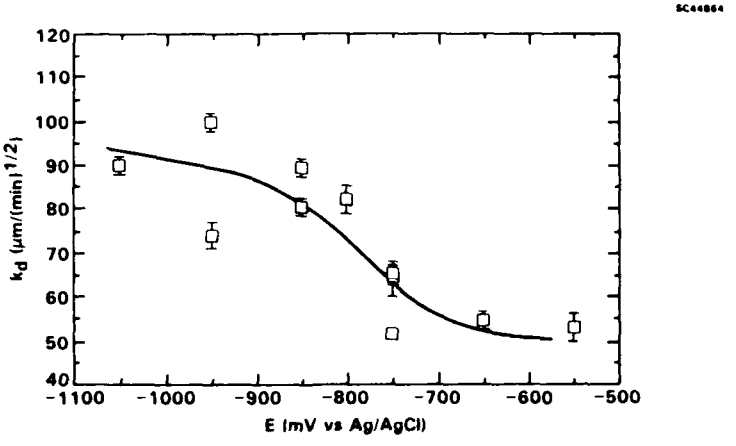

Fig. 4 Potential dependence of the disbonding rate constant, K_d.

The development of the circular "microblisters" has not been previously reported. They are not observed by light optics. It was initially believed that they were due to local swelling of the polymer resulting from electroosmotic influx as the term "microblister" indicates. A definite volume change would result if blistering/electro-osmotic swelling occurred. For this explanation to be correct, microblisters would be optically detectable using a microscope with Nomarsky contrast or by examining the polymer surface with an interferometric microscope. Both of these techniques have been tried, but neither of them was able to detect any surface distortion of the polymer that could have been associated with microblisters. In addition, the microblisters remain after dry out and partial readhesion of the coating after storage for 24 hours under vacuum.[2]

The current hypothesis is then that an irreversible localized change in the elastic properties of the polymer occurs possibly as a result of alkaline hydrolysis due to reactions similar to those described in the literature for other polymers.[9-12] To evaluate the role of alkaline products on the acoustic properties of the polymer films, a drop of 1 M NaOH was placed on the polymer film for one minute. The region below the drop turned a straw color. The region was wiped with a dampened cotton swab and the colored layer was removed leaving no optical evidence that any change in the polymer had occurred. However, examination with the SAM clearly showed a contrast change in the region that had been exposed to the NaOH (Fig. 5). An additional observation of the behavior of the circular features in the disbond zone suggest that the features are due to polymer degradation rather than electroosmotic blister formation. The fringes seen in the microblisters mark changes in the acoustic path-legnth (see micrographs in references 1-5). For a given thickness of the polymer, there is always the same maximum number of fringes for the larger microblisters indicating that the height of the blisters is limited by the polymer thickness although lateral spreading occurs.

Figure 6 summarizes an initial hypothesis concerning how the disbonding process occurs. The cathodic reaction is driven by the potential between the electrolyte and the steel. Castle and Watts[14] have previously shown that an iron oxide/polymer interphase exists between the bulk polymer and the metal oxide substrate for this particular class of coatings. The diffusion of the reactants into the interphase region at

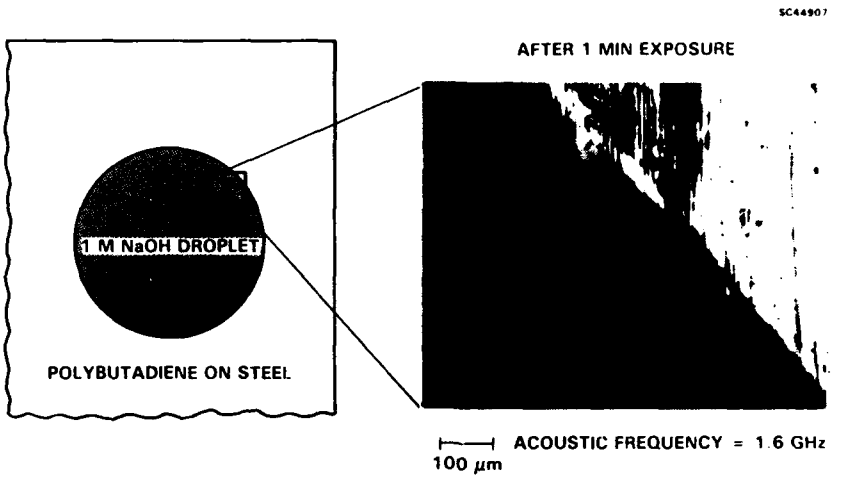

Fig. 5 Acoustic micrograph illustrating alteration of the hydroxy-terminated polybutadiene by exposure to 1.0 M NaOH.

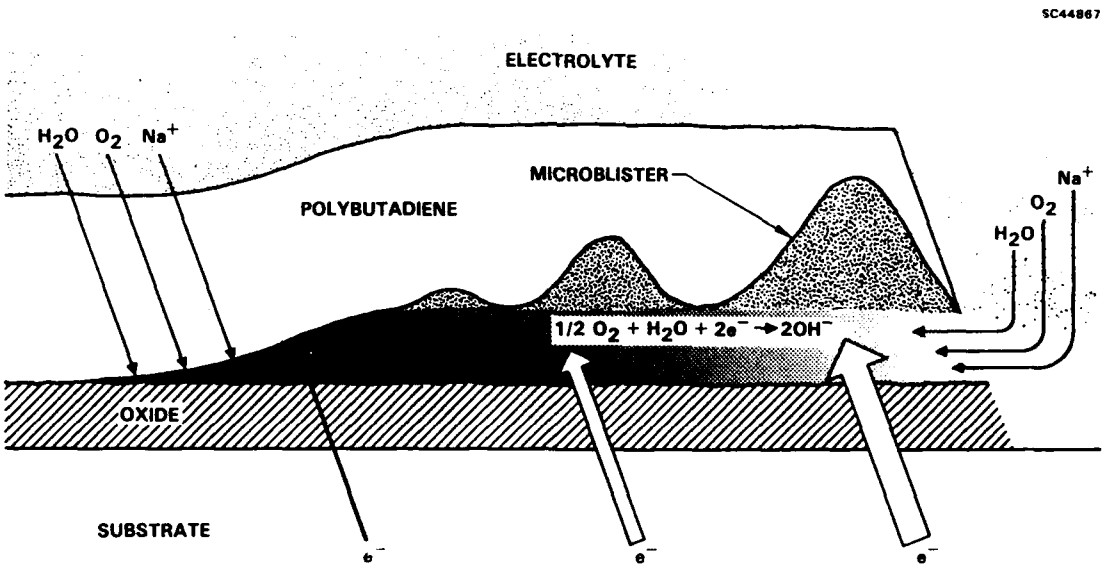

Fig. 6 Model for the polymer degradation process.

the leading edge of the disbond is consistent with the observation of a $\sqrt{t}$ time dependence. The reactants, water, oxygen and sodium ion, diffuse in from the scribe mark and

through the polymer. A set of rate equations for these reactions has been formulated by Thornton et al.[15] They solved the equations under a simplifying set of assumptions showing that the rate of advance of the disbond was proportional to $\sqrt{t}$. The electrochemical reactions reduce oxygen to form OH^- whose charge is balanced by the influx of hydrated Na^+ ion. Charge transport by diffusion of the hydrated cation to the interphase due to osmosis along with changes in the surface energy associated with reduction of surface oxides (see Section 4.2) provide the mechanical pressure to rupture the interfacial bonds and drive the disbond along the interface.

The nature of the oxide/coating interphase and not just the chemistry of the coating references the disbonding process. As an illustration, cathodic disbonding kinetics were also obtained for different surface treatments. The results in terms of values of K_d and t_o (Eq. (1)) appear in Table 2. A highly polished surface pretreatment exhibits accelerated disbonding as compared to the standard polished and degreased (P+D) specimen. The initiation time for this specimen, however, is somewhat longer as compared to that for the P+D specimen (Table 2). The increase in K_d for the highly polished specimen no doubt relates to the shorter, less tortuous diffusion path for oxygen and Na^+ along the disbond away from the scribe. Although the nitric acid treated specimen has a longer initiation time to, it exhibits a relatively rapid disbond rate as measured by K_d. This indicates that the nitric acid treatment gives a less stable oxide under cathodic conditions. The sample having a surface treated with inhibited HCl and treated with the organo-titanate adhesnion promoters (LICA #38) exhibit a halving in the disbond rate and an increase in t as compared to the P+D specimen (see Table 2).

4.2 Potential-Dependent Surface Energy of Steel Under Cathodic Disbond Conditions

As shown by the SAM data and previous work reported in the literature, the cathodic conditions which exist in the disbonding crevice degrade the polymeric material at the interface which clearly contributes to irreversible degradation of adhesion (Coating degradation model or Castle and Watts (14) type I mechanism). Cathodic dehydration or alteration of the oxide/coating interphase may also play a role in the disbonding process. The presence of the high pH regions at the coating/metal interface may ultimately lead to the dissolution of the metal oxide, particularly under reducing

Table 2
Cathodic Disbonding
Effects of Different Sample and Surface Treatments

SPECIMEN ID	SPECIMEN/SURFACE TREATMENT*	K_d ($\mu m/\sqrt{min}$)	t_o (min)
65	P+D	82±3	4
96	POLISHED <1 μm	108±4	25
53	P+D/HNO_3	68±2	71
41	P+D/INH. HCl	52±2	26
45	P+D/LICA IN POLYMER	52±1	2
46	P+D/LICA ON SURFACE	41±2	27

*GLOSSARY OF TERMS

P + D	POLISHED AND DEGREASED
HNO_3	STEEL OXIDIZED WITH HNO_3
INH. HCl	STEEL CLEANED WITH HCl CONTAINING INHIBITOR
LICA	KENRICH ORGANOTITANATE COUPLING AGENT #38

conditions as shown by Ritter[16] (Castle and Watts[14] type III mechanism). However, it is unclear whether these are necessary conditions for the cathodic disbonding. The fact that a rise in the rate constant occurs over a relatively narrow potential region as shown in Fig. 4 does suggest that oxide reduction may play a role in the disbonding process. Elucidation of these details requires observation of the role of electrochemical reactions on the chemistry and surface energy of the steel surface under conditions simulating the disbonding environment. In addition there exists the Koehler[17] mechanism of interfacial failure (Castle and Watts type II mechanism) which has not received the attention that the other mechanisms have. Koehler[17] poses the question: are there chemical and electrochemical conditions under which water displaces foreign material (in this case the coating) from the metal surface as occurs in alkaline cleaning? Do conditions exist which provide the surface with a greater affinity for water as compared to organics? These remain valid questions. The work presented here attempts to quantify the tendency of water to displace organics from steel as a function of potential by first evaluating the relative tendency of steel to be wet by water as a function of potential.

The relative water wetting of steel was evaluated from the changes in the wetting tension γ, as a function of potential. When a cylindrical specimen is immersed in a liquid of surface tension γ_l (Fig. 7), the force F on the specimen is

$$F = mg + P\gamma_l\cos\theta - \rho_l g\pi r^2 d \qquad (2)$$

where the parameters in the above equation are defined in Fig. 7. The wetting tension, γ provides a measure of the ability of the liquid to bond to the metal and is defined as:

$$\gamma = \gamma_l\cos\theta = (F - mg + \rho_l g\rho^2 d)/P \qquad (3)$$

Where γ_l is the surface tension of the liquid/air interface and θ is the liquid/metal contact angle. F and hence γ are readily measured using the apparatus shown in Fig. 2.

Figure 8(a) shows the potential dependence for γ for a steel cylinder that had been polished with 600 grit SiC and etched in concentrated HCl before measuring the wetting forces or wetting tension in 0.5 M NaCl. It should be pointed out that the γ vs potential curves are irreversible. Once increased wetting occurs (a rise in γ) with applied cathodic potential, γ does not decrease upon reversing the potential. This may be a result of the fact that adsorbed airborne organics are irreversibly displaced by the water upon ramping up the potential.

Although the curve for γ as a function of potential (Fig. 8(a)) looks remarkably similar to the curve for the disbonding kinetics, K_d vs potential (Fig. 4(b)); the potential, E_w, where γ shows a sharp rise in 0.5 M NaCl is somewhat cathodic to that potential where K_d increases. The results clearly show that HCl-etched steel becomes more wettable by water for potentials more negative than -800 mV vs Ag/AgCl (Fig. 8).

The increase in γ may be associated with the onset of hydrogen formation as illustrated by the current density obtained during the wetting experiment and plotted vs potential in Fig. 8(b). Between the open circuit or corrosion potential of -630 mV and a potential of -800 mV, the diffusion limited oxygen reduction dominates to give a current of 10 $\mu A/cm^2$ which is more or less independent of potential. However, at -800 mV vs Ag/AgCl, the formation of hydrogen occurs more rapidly than the oxygen reduction.

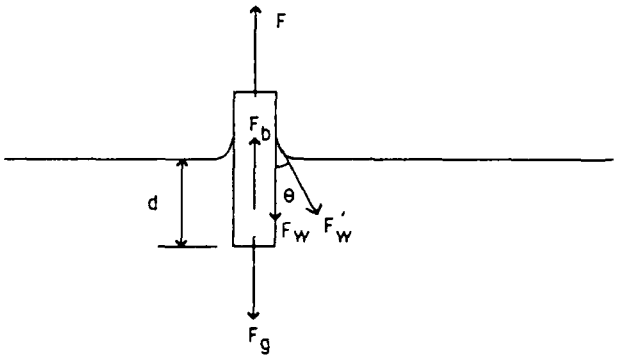

$F = F_g + F_w + F_b$

$F_w' = P\gamma_l$ = wetting force of liquid

$F_w = P\gamma = P\gamma_l \cos\theta$ = wetting force

$F_g = mg$ = gravitational force

$F_b = \pi r^2 d\rho$ = buoyancy

P = perimeter of the sample
r= radius of cylindrical sample
d = immersion depth
g = gravitational constant
ρ = liquid density
γ_l = surface tension of the liquid
γ = wetting tension

Fig. 7 Schematic showing the forces present during the wetting balance experiment.

Predomination of current due to hydrogen formation over oxygen reduction coincides with the onset of enhanced wetting of the steel. The onset of hydrogen reduction can relate to increased hydrophilic behavior (increased γ) by three possible mechanisms:

1. Hydrogen evolution results in an increase in the rate of formation of OH^- which promotes displacement of organic contaminants by the aqueous phase.

2. Onset of hydrogen reduction is coincident with the reduction or reductive dissolution of hydrophobic oxides which increase hydrophilic behavior.

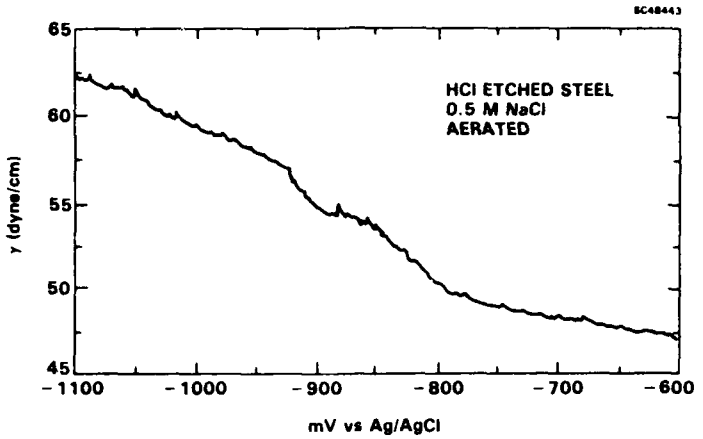

(a)

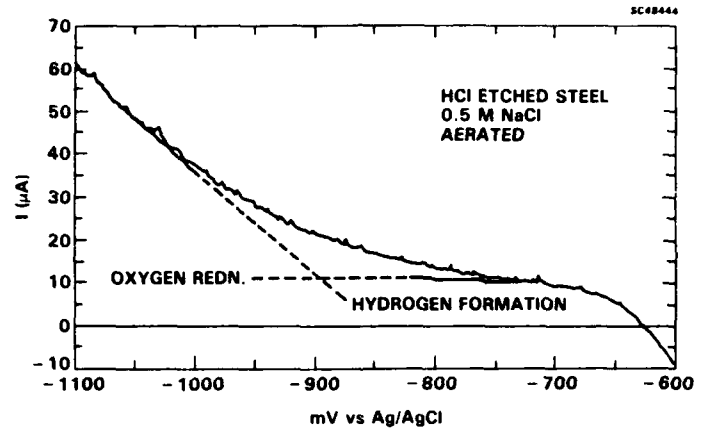

(b)

Fig. 8 Potential dependence for (a) the wetting tension, γ, and (b) the current density of steel in 0.5 M NaCl. The potential was varied at a constant rate of 0.5 mV/s from just above the open circuit potential to the -100 mV.

3. Adsorption of atomic H promotes water affinity for the surface and hence increases γ.

Figure 9 shows plots for the change in wetting tension, $\Delta\gamma$, as a function of potential for the steel specimen immersed in 0.5 M NaOH (pH ~ 13.6) for duplicate experiments. The potential, E_w, defined as the potential where γ reaches 1/2 its maximum value is at -910 and -975 for these two experiments. Results of E_w as a function of pH for the steel immersed in the different solutions in Table 1. appear in

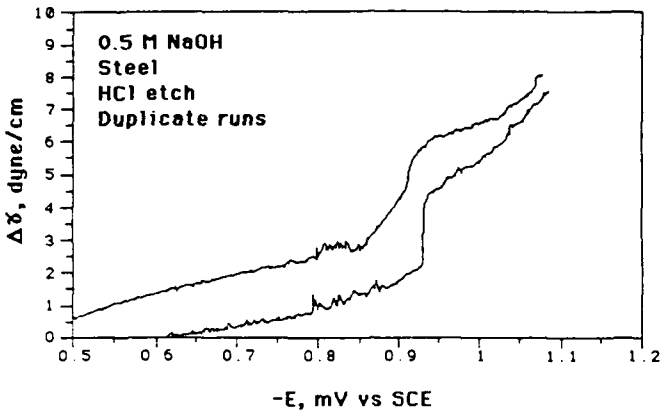

Fig. 9 Change in the wetting tension, $\Delta\gamma$, as a function of cathodic polarization in 0.5 M NaOH for two HCl-etched steel specimens.

Fig. 10. The scatter in the data make it difficult to spot any influence of pH. It is likely that the pH at the metal surface in the unbuffered solutions depends little on the bulk concentration. Rather the cathodic polarization governs the pH in that the pH depends entirely on the flux of the applied current.

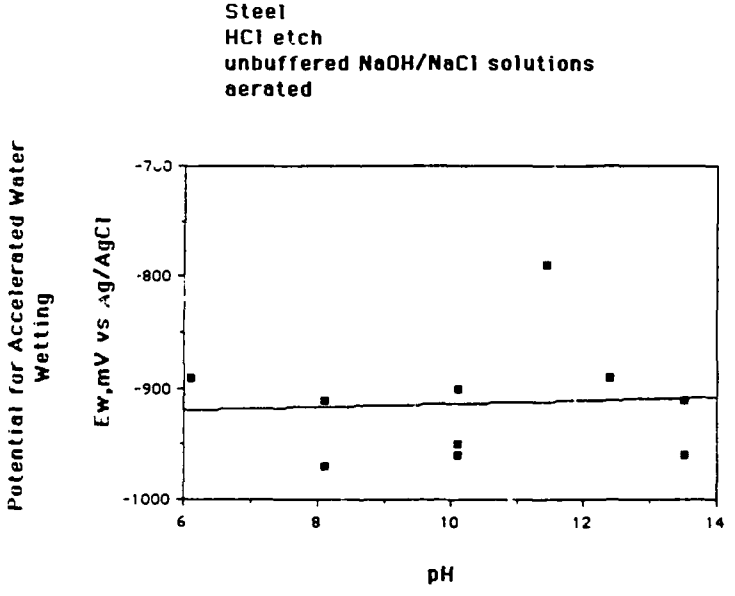

Fig. 10 pH dependence for the potential E_w where accelerated wetting occurs.

It was therefore considered more meaningful to examine the wetting behavior of the steel in a buffered electrolyte under galvanostatic conditions. Figure 11(a) shows the wetting behavior for a steel rod etched in concentrate HCl and exposed to a buffered 0.1 M H_3BO_3 adjusted to pH 9.6 with NaOH additions. With a galvaniostatic polarization of -74 $\mu A/cm^2$, the potential rapidly rises to -550 mV vs Ag/AgCl and γ rises slowly. Increasing the applied current to -220 $\mu A/cm^2$ causes a sharp rise in the potential to -900 mV vs Ag/AgCl and a nearly simultaneous rise in the wetting tension by about 15 dyne/cm (Fig. 11(a)).

For several experiment a passive film was grown on the specimen in the borate buffer at an anodic potential of 0 V vs Ag/AgCl for 4 min. The specimen was then polarized galvanostatically at -220 mV. The resulting time dependence for $\Delta\gamma$ and the potential, E, appear in Fig. 11(b). At 35 s, the potentiostatic polarization at 0 V is ceased. The potential equilibrates to and open circuit value of -200 mV with virtually no change in the wetting tension γ (Fig. 11(b)). At 160 s, the cathodic current is applied and the potential decreases immediately to -500 mV and then slowly changes until it reaches a value of -750 mV (note arrow in Fig. 11(b)), whence it rapidly decreases to a steady value of -900 mV (Fig. 11(b)). Based on the work of M. Cohen[18], the transition between the -500 mV and -900 mV vs Ag/AgCl represents a transformation of the oxide from a cation deficient γ - Fe_2O_3 to a Fe_3O_4 oxide. The transformation from a +3 oxide to a reduced oxide for iron has been more recently reported by Biwer et al using the in situ optical method of second harmonic generation (SHG).[19] The in situ SHG signals are consistent with the formation of $Fe(OH)_2$ from the original Fe_2O_3 passive film in aerated borate buffer starting at potentials of -750 mV (Ag/AgCl) where wetting has been observed here to occur. Since work reported here was done in oxygenated solutions, the reduction to the metallic state could not be completed at the current density used. Note that the onset of accelerated wetting occurs, as evidenced by a rapid rise in γ at 225 s in Fig. 11(b), only after the transformation to the reduced oxide phase is completed with a corresponding decrease of the potential to values more negative than -750 mV vs Ag/AgCl. This experiment was repeated many times with the result that an inflection in the potential current curve at -750 mV coincides with an increase in the wetting tension γ. The more reduced oxide appears, therefore, to have an enhanced affinity for water. It is not clear whether the enhanced wetting results from the transformation of the oxide to the reduced state which may be inherently more hydrophilic, or whether the reduced

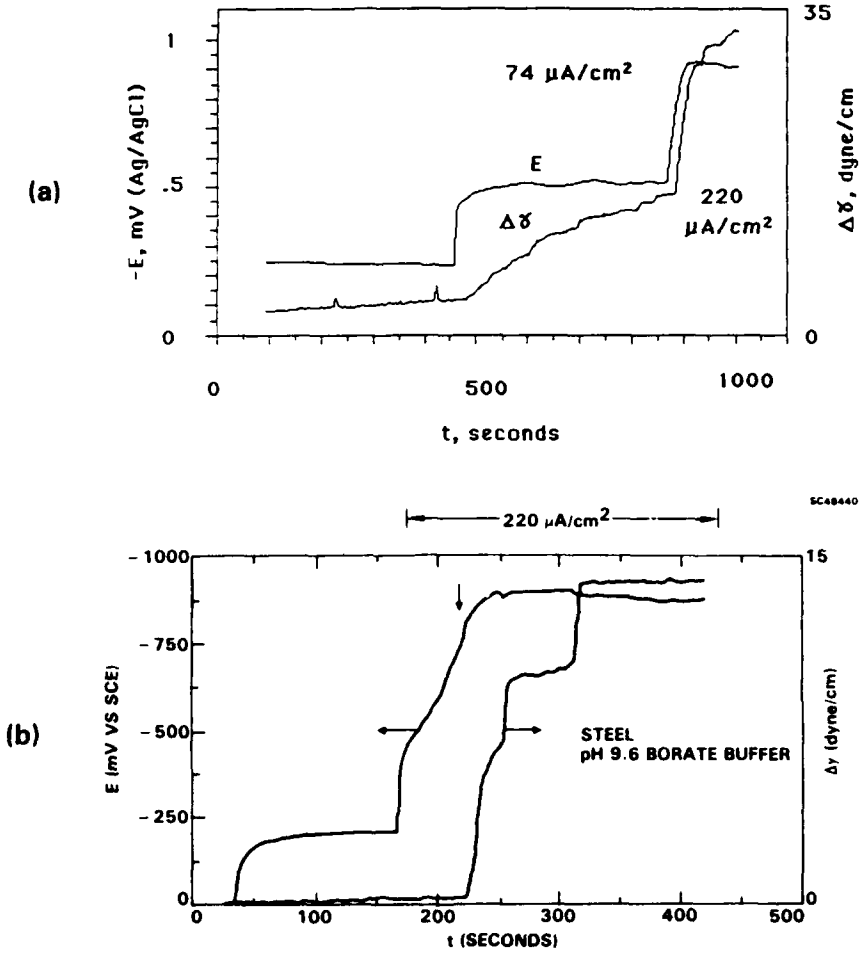

Fig. 11 Change in wetting tension, $\Delta\gamma$, and potential, E as a function of time during galvanic polarization of mild steel in pH 9.6 borate buffer: (a) sample etched in HCl, (b) sample prepolarized for 3.7 min. at 0 V vs Ag/AgCl in the 0.1 M pH 9.6 borate buffer.

oxide is more hydrophillic as a result of greater hydrogen adsoption associated with the observed increase in hydrogen evolution reaction. Nevertheless, enhanced hydrophilicity correlates with oxide reduction.

4.3 Surface Analysis of Cathodically Polarized Steel Surfaces in Alkaline Environments

The potential dependence for the wetting of the steel suggests that mild steel achieves enhanced hydrophilic properties upon cathodic transformation of the surface

oxide from a +3 oxide to more reduced state which is completed around -750 mV vs Ag/AgCl in pH 9.6 borate buffer. This enhanced wetting correlates with accelerated cathodic disbonding. In order to obtain a more precise identification of the chemistry of the oxide which exists on the metal surface at the potentials in question, surface analyses of steel treated in alkaline environments at open circuit and under cathodic polarization were pursued. Although related work has been previously reported,[10-14] all the previous work entailed an air transfer of the specimen to the UHV chamber for analysis. Oxide reduction was reported only under extreme conditions of high cathodic polarization. Castle and Watts[8] applied -1500 mV vs SCE and observed partial reduction at the disbond front with the remainder of the region reoxidized. The objective of the surface analysis presented here is to characterize the extent of reduction or partial reduction of steel in alkaline environments typical of the disbond zone encountered during corrosion polymer-coated steel. To limit oxidation of reduced species, the work reported here resulted from direct transfer from the electrochemical conditioning cell to the chamber as described in Section 3.3. Some problems were encountered as a result of alkaline attack of the cell material with the resulting presence of breakdown products (silica) from the cell depositing on the sample surface. The results reported here must, therefore, be considered preliminary in nature. The experiments will be repeated with a redesigned cell containing no glass composites.

Figures 12(a) and 12(b) show the Auger (AES) spectra for the steel specimen before exposing to the test solution. It has a thin oxide film (Fig. 12(a)) which is readily removed by Ar ion etching as shown by the decrease in the O lines and increase of the Fe lines after a 100 s Ar ion etch (Fig. 12(b)). A significant contamination of the initial surface by C is also noted (Fig. 12(a)). Upon exposure to the 1.0 M NaOH solution with no cathodic polarization, the specimen becomes covered with an oxide rich in silica, and Na (Fig. 13). Two oxygen lines define the x-ray photoelectron spectrum (XPS) for this surface (Fig. 14). The low energy line is at 532.5 eV with the high energy line attributable to OH^- at 534.5 eV. The iron line is very weak since quantities of silica and NaO apparently cover the surface. The iron line has a maximum at 712.4 eV (Fig. 15).

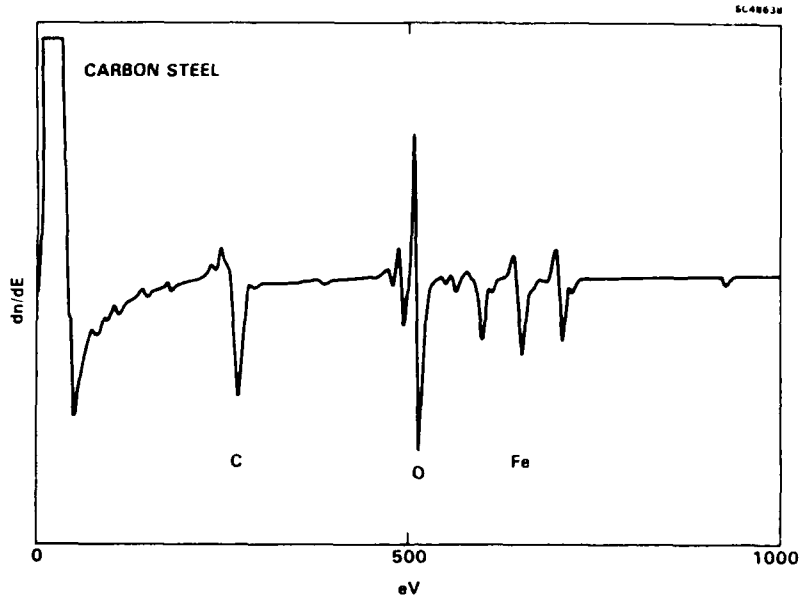

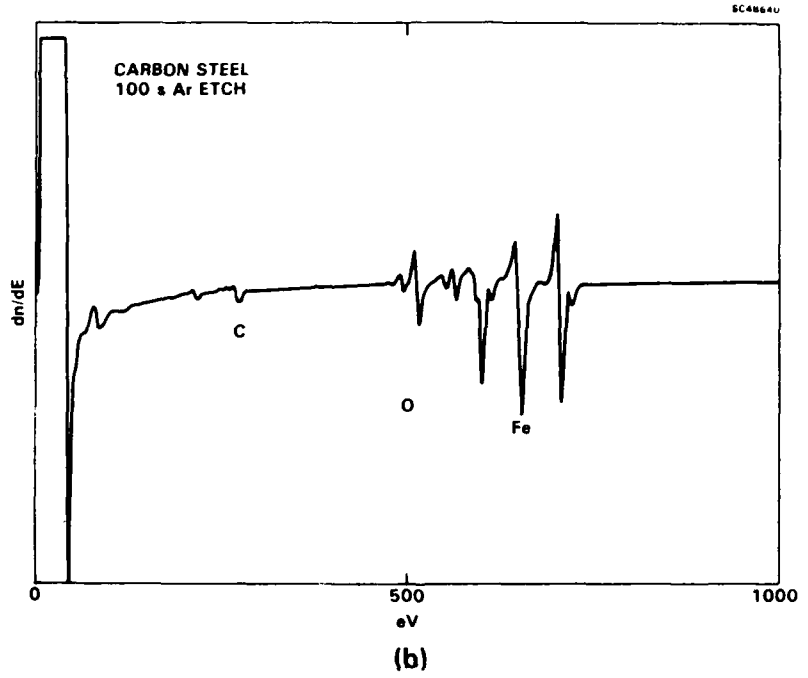

Fig. 12 Auger electron spectrum for (a) a polished and air aged steel specimen before exposure to 1 M NaOH, and (b) after ion etching.

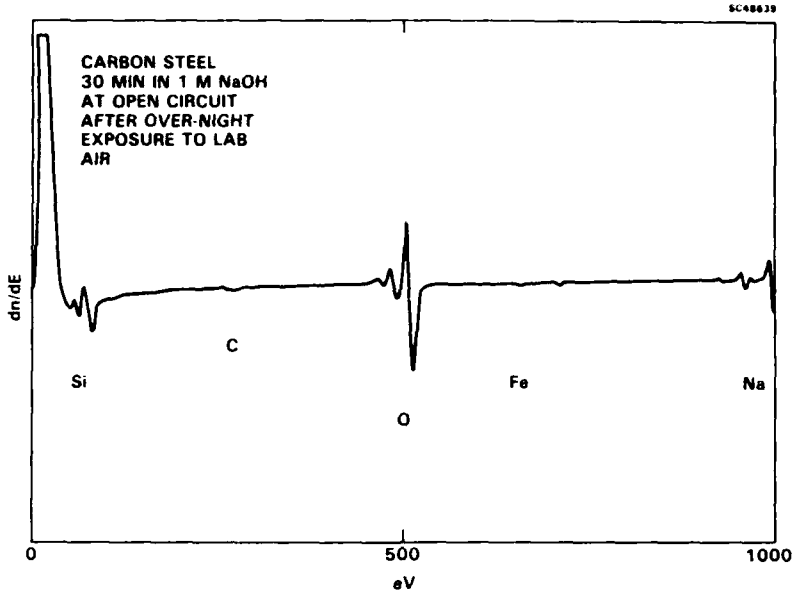

Fig. 13 Auger electron spectrum for a polished and air aged steel specimen after exposure to deaerated 1 M NaOH.

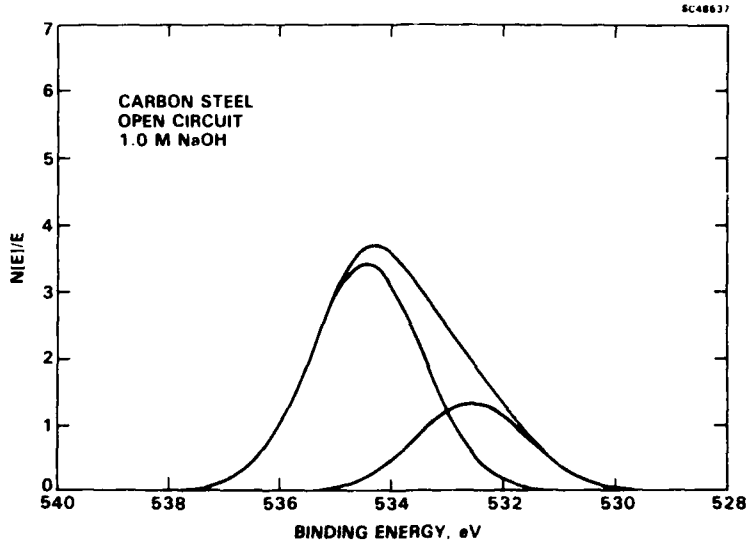

Fig. 14 Oxygen 1s X-ray photoelectron spectrum for the specimen of Fig. 13.

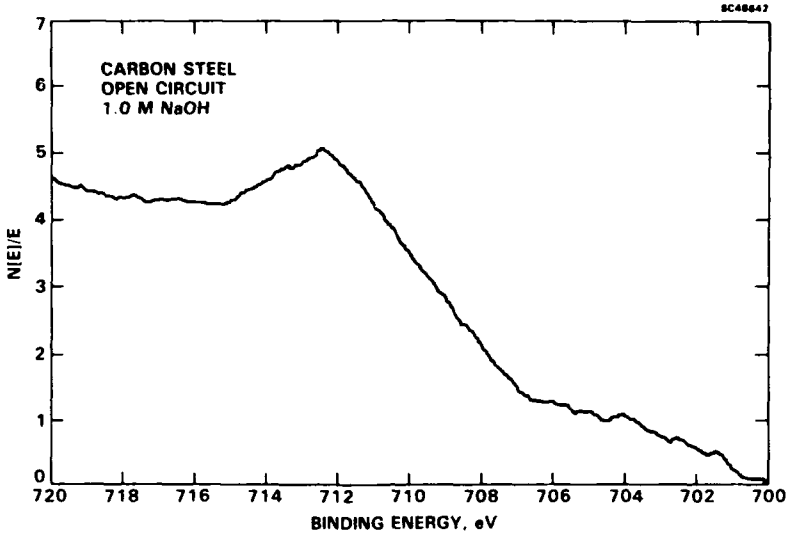

Fig. 15 Iron 2p X-ray photoelectron spectrum for the specimen of Fig. 13.

The sample polarized at -745 mV in 1 M NaOH (at potentials just positive to the onset of cathodic disbonding (see Fig. 4)) exhibits a surface containing oxygen predominantly in the OH^- chemical state as shown by the Oxygen XPS (Fig. 16). Again, the large quantity of silica debris on the surface results in a very weak Fe XPS spectrum (Fig. 17) which can be attributed to a Fe_3O_4 species.

The specimen treated at -1032 mV (6 μA) in the 1 M NaOH solution was rinsed before obtaining XPS spectra in the UHV and Ar etched to remove some of the silicon containing debris. As for the other treatments, the oxygen line shows that the surface oxides exists predominantly as hydroxide with some oxide (the high energy peak dominates) (Fig. 18). The iron XPS spectrum shows a maximum for Fe metal at about 707.6 eV and for Fe_3O_4 at 711 eV (Fig. 19).

For all treatments in 1.0 M NaOH, large quantities of silica up to 1000Å based on Ar etching covered the surface making the observation of the underlying oxide structure difficult at best and questionable in interpretation in any case.

Therefore, it was decided to cathodically prepare the specimen in a less alkaline solution (lower activity of OH^-). Upon treating the specimen in 0.001 M NaOH

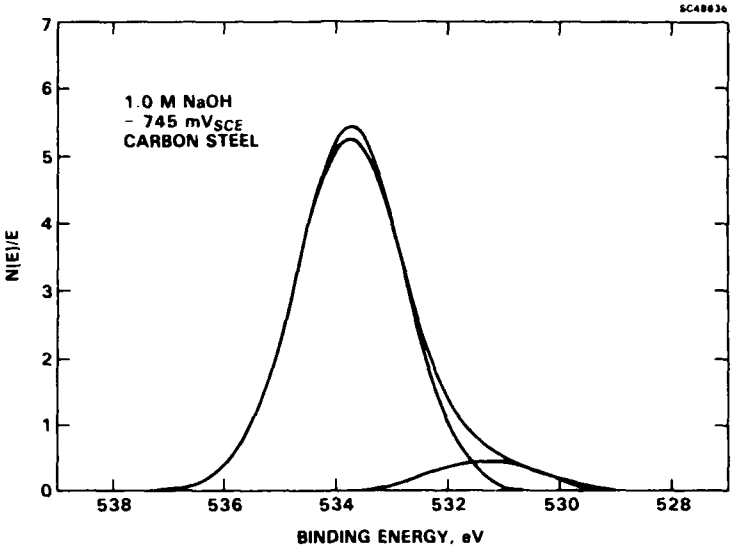

Fig. 16 Oxygen 1s X-ray photoelectron spectrum for steel exposed to deaerated 1.0 M NaOH at -745 mV vs SCE (-700 mV vs Ag/AgCl).

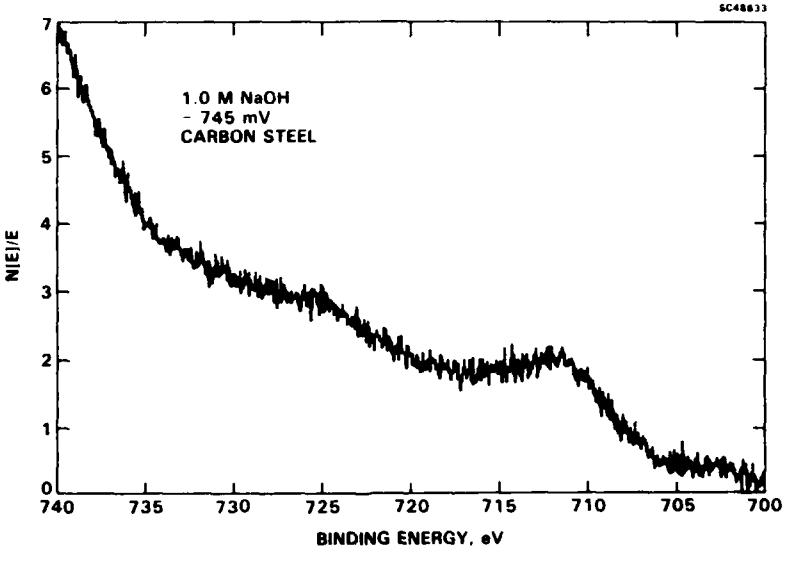

Fig. 17 Iron 2p X-ray photoelectron spectrum for steel exposed to deaerated 1.0 M NaOH at -745 mV vs SCE (-700 mV vs Ag/AgCl).

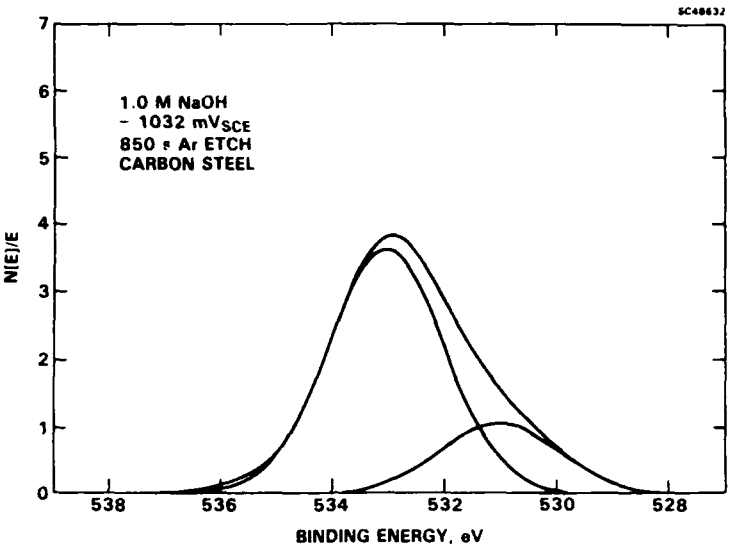

Fig. 18 Oxygen 1s X-ray photoelectron spectrum for steel exposed to deaerated 1.0 M NaOH at -1032 mV vs SCE (-987 mV vs Ag/AgCl).

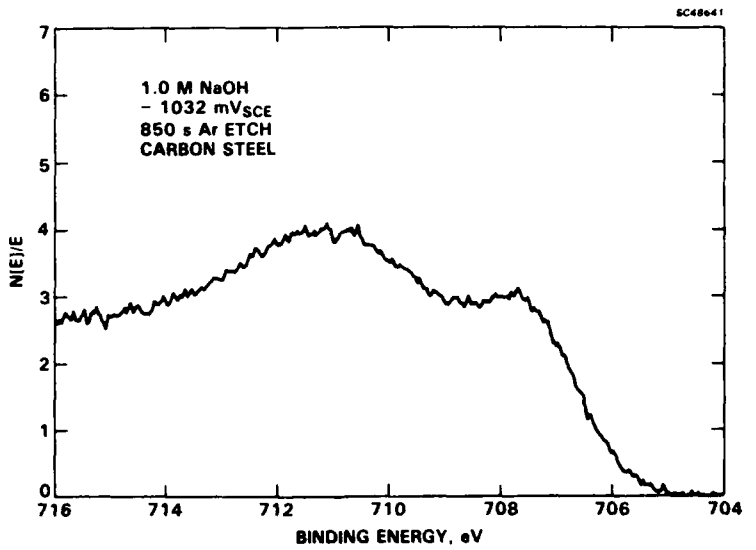

Fig. 19 Iron 2p X-ray photoelectron spectrum for steel exposed to deaerated 1.0 M NaOH at -1032 mV vs SCE (-987 mV vs Ag/AgCl).

an even larger quantity of silica was observed on the surface than observed after the use of the 1.0 M NaOH test solutions as evidence from AES spectra. Figure 20 shows time dependence of the intensity ratio for the Fe to Si Auger peaks as a function of sputtering time for the sample treated at 1 V in 0.001 M NaOH. As can be seen, even after sputtering for 3200 s, the Fe spectrum remains weak due to the coverage of the surface by silica. The fact that a large quantity of silica deposited on the surface even under milder conditions of alkalinity suggested that degradation of the cell resulted in hide-out of silica from previous use of the 1 M NaOH. The likely component of the sample prepration cell which is degraded to produce the high volume of silica is the glass/teflon composite cell body. For future work, this component will be made from a non-glass containing material.

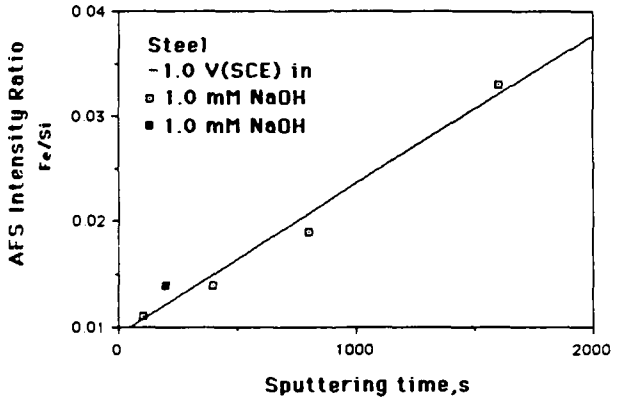

Fig. 20 Intensity ratio for the Fe/Si Auger lines as a function of the time of Ar ion etching for the sample exposed to 0.001 M NaOH at -1000 mV vs SCE (-955 mV vs Ag/AgCl).

With removal of the Si by Ar etching to expose the compounds assumed to be present at the metal/electrolyte interface during the pretreatment by cathodic polarization, the Fe and O spectra appear as shown in Figs. 21 and 22, respectively. The Fe spectrum appears to be that for Fe_3O_4 and metallic Fe while the oxygen spectrum contains a large component of OH^-. The maximum for the low energy iron oxide peak is at 711.2 eV. It must be noted that the energy for this particular transition decreases with decreasing electrochemical pretreatment potential (increasing cathodic potential) as shown in Fig. 23.

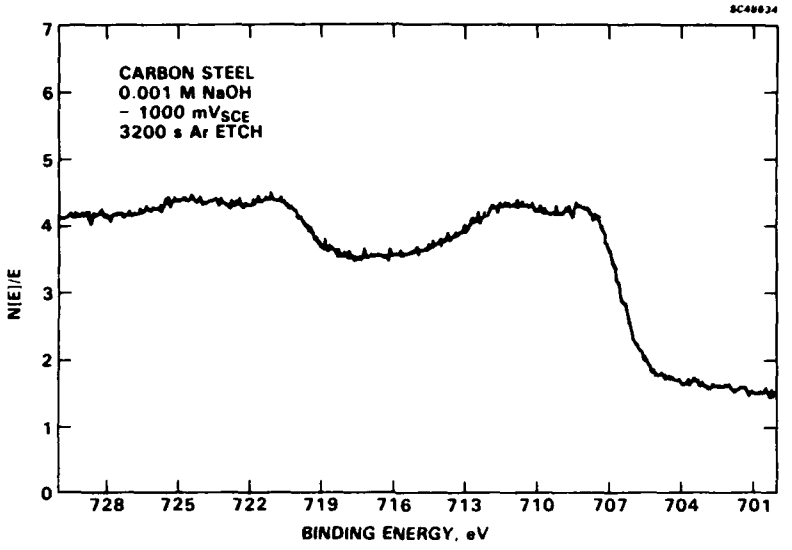

Fig. 21 Iron 2p X-ray photoelectron spectrum for steel exposed to deaerated 0.001 M NaOH at -1000 mV vs SCE (-955 mV vs Ag/AgCl).

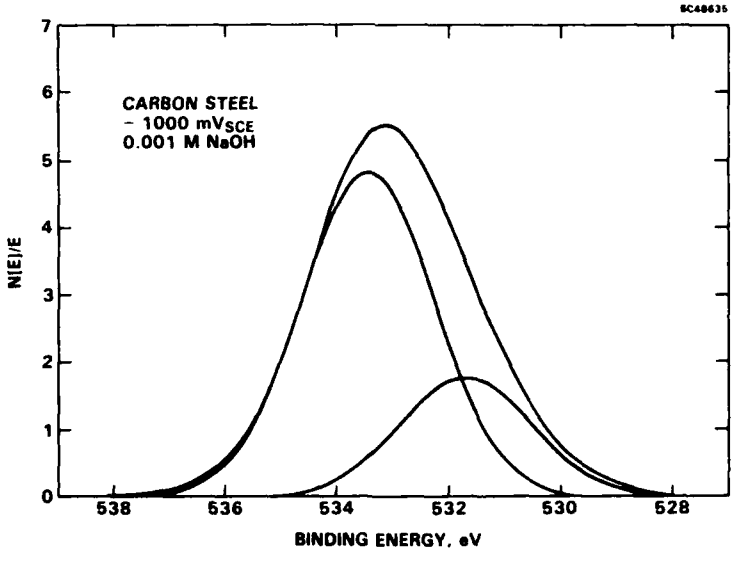

Fig. 22 Oxygen 1s X-ray photoelectron spectrum for steel exposed to deaerated 0.001 M NaOH at -1000 mV vs SCE (-955 mV vs Ag/AgCl).

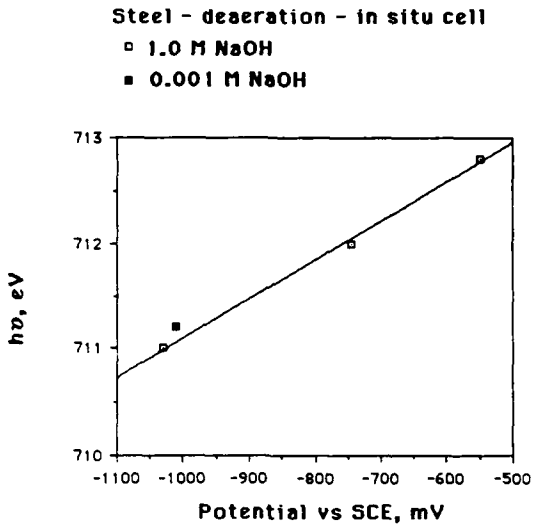

Fig. 23 Energy for the maximum in the low energy peak of the Fe oxide 1s X-ray photoelectron spectrum as a function of polarization in the in situ cell.

It must be reiterated that these experiments will be repeated with a new cell since the cell degradation products apparently contaminated the sample surfaces. The results must be considered preliminary at this time, and no definite conclusions can be made. Nevertheless, the iron oxide apparently changes character becoming more reduced upon cathodic polarization in the alkaline environments (Fig. 23). Indeed, for the polarization at -1 V or more, the presence of metallic iron can be detected possibly as a result of the thinning of the metal oxide.

5.0 SUMMARY

The in situ acoustic microscopic examination of cathodic disbonding of the organic coatings from steel allowed both the kinetics of the disbonding process as well as the consequent attack of the alkaline solution on the polymer coating to be accurately assessed. The kinetic analysis showed a $\sqrt{t}$ behavior for the disbonding rate as is consistent with previous theories. Acceleration of the disbonding occurs at -750 mV vs Ag/AgCl in the 0.5 M NaCl environment. The resulting alkaline solution formed in the disbonded region attacks the polymer at numerous localized spots within the disbonded zone. The polymer degradation is irreversible. Drying of the film may produce some readhesion of the disbonded zone, but the localized degradation in the mechanical properties of the polymer remains.

Cathodic polarization enhances the ability of alkaline and neutral electrolytes to wet steel. This phenomenon may also contribute to the loss of adhesion of organic films from steel surfaces. The enhanced wetting as a result of cathodic polarization does not result from the formation of sodium hydroxide from the cathodic oxygen reduction, since the effect was observed in a buffered borate solution. The enhanced wetting under cathodic polarization appears to result from the reduction of the metal oxide to a lower valent and more hydrophilic oxide. This chemical change can contribute to the loss of adhesion which occurs under cathodic polarization. Oxide reduction is consistent with preliminary XPS analysis.

6.0 FUTURE WORK

Work for the coming contract year will entail completing the XPS and AES surface analysis of steel maintained at cathodic potentials in alkaline environments using a modified cell so as to eliminate silica contamination of the sample. The wetting work will also continue in parallel. The wetting tension of steel with a surface covered by adsorbed acidic or basic polymers from acidic or basic solvent as described by Fowkes[20] will be determined as a function of cathodic polarization. In this way, the acid/base properties of the actual cathodically polarized steel surface will be determined. The results will allow identification of specific polymer/metal interactions that inhibit water displacement of the polymer in the presence of an applied cathodic polarization. This will lead to a better specification of organic polymers resistant to cathodic displacement by corrosive electrolytes.

REFERENCES

1. M. Kendig, R. Addison, and S. Jeanjaquet, "Environmental Integrity of Coating/ Metal Interface," Annual Progress Report No. 1 for the Period February 1 through January 31, 1988, Contract No. N00014-87-C-0075, January 1988.
2. R.C. Addison, Jr., M.W. Kendig and S.L. Jeanjaquet, "In Situ Measurement of Cathodic Disbonding of Polybutadiene Coating on Steel," Acoustic Imaging 17 (1988).
3. R.C. Addison, Jr., M.W. Kendig and S.L. Jeanjaquet, "Acoustic Microscopic Evaluation of Hydroxy-Terminated Polybutadiene on Steel," Proc. Ultrasonic Symposium of the IEEE, Chicago, 1988.
4. M. Kendig, R. Addison and S. Jeanjaquet, "Acoustic Microscopic Evaluation of Hydroxy-Terminated Polybutadiene on Steel," extended abstract, Proceedings of the 174th Meeting of the Electrochemical Society, October 1988.
5. M. Kendig, R. Addison and S. Jeanjaquet, "The Mechanism of Cathodic Disbonding of Hydroxy - Terminated Polybutadiene on Steel from Acoustic Microscopy and Surface Energy Analysis," extended abstract of a paper to be presented at Advances in Corrosion Protection by Organic Coatings, to be held April 1989, Christ's College, Cambridge, UK.
6. M. Kendig and F. Mansfeld, "Lifetime Prediction of Organic Coatings on Steel," Materials Research Society Proceedings 125, 293 (1988).
7. M. Kendig, S. Tsai and F. Mansfeld, Materials Performance 23(6), 37 (1984).
8. J.B. Lumsden and P.J. Stocker, "Effect of Transfer Technique Between Solution and UHV on the Chemistry of Passive Films on Well-Defined Stainless Steel Surfaces,"
9. J.S. Hammond, J.W. Holubka, J.E. DeVries and R.A. Dickie, Corrosion Sci., 21(3), 239 (1981).
10. J.W. Holubka and R.A. Dickie, J. Coat. Tech. 56(714), 43 (1984).
11. J.W. Holubka, J.E. deVries and R.A. Dickie, Ind. Eng. Chem. Prod. Res. Dev. 23, 63 (1984).
12. J.W. Holubka, J.S. Hammond, J.E. DeVries and R.A. Dickie, J. Coat. Technol. 52(670), 63 (1980).
13. M.W. Kendig and T.A. Fadner, I and EC Fundamentals 24, 50 (1985).
14. O. Murphy and J.S. Wainright, J. Electrochem. Soc.,

14a J.E. Castle and J.F. Watts, I&EC Product Research and Development 24, 361 (1985); and J.F. Watts, J.E. Castle, J. Materials Science 18, 2987 (1983).

15. J.S. Thornton, R.E. Montgomery and J.F. Carter, "Failure Rate Model for Cathodic Delamination of Protective Coatings," NRL Memorandum Report, Contract No. N00014-83-C-2258 (1985).

16. J. Ritter, J. Coatings Technol. 54, 695 (1982).

17. E.L. Kohler, Corrosion 40(1), 5 (1984).

18. M. Cohen, "The Passivity and Breakdown of Passivity on Iron," in Passivity of Metals, edited by R. Frankenthal and J. Kruger, Corrosion Monograph Series, Electrochemical Soc., 1978.

19. B.M. Biwer, M.J. Pellin, M.W. Schauer and D.M. Gruen, Langmuir 4, 121 (1984); and B.M. Biwer, M.J. Pellin, M.W. Schauer and D.M. Gruen, Surface Science 176, 377 (1986).

20. F. Fowkes, "Pigment-Matrix Interactions," in Corrosion Control by Organic Coatings, H. Leidheiser, Jr., ed., Science Press, Princeton, 1979.